© 2020. Published by The Company of Biologists Ltd | Development (2020) 147, dev192518. doi:10.1242/dev.192518

Snx3 is important for mammalian neural tube closure via its role in canonical and non-canonical WNT signaling

Heather Mary Brown[1,2], Stephen A. Murray[3], Hope Northrup[4], Kit Sing Au[4] and Lee A. Niswander[2,*]

ABSTRACT

Disruptions in neural tube (NT) closure result in neural tube defects (NTDs). To understand the molecular processes required for mammalian NT closure, we investigated the role of *Snx3*, a sorting nexin gene. *Snx3*$^{-/-}$ mutant mouse embryos display a fully-penetrant cranial NTD. *In vivo*, we observed decreased canonical WNT target gene expression in the cranial neural epithelium of the *Snx3*$^{-/-}$ embryos and a defect in convergent extension of the neural epithelium. *Snx3*$^{-/-}$ cells show decreased WNT secretion, and live cell imaging reveals aberrant recycling of the WNT ligand-binding protein WLS and mis-trafficking to the lysosome for degradation. The importance of SNX3 in WNT signaling regulation is demonstrated by rescue of NT closure in *Snx3*$^{-/-}$ embryos with a WNT agonist. The potential for SNX3 to function in human neurulation is revealed by a point mutation identified in an NTD-affected individual that results in functionally impaired SNX3 that does not colocalize with WLS and the degradation of WLS in the lysosome. These data indicate that *Snx3* is crucial for NT closure via its role in recycling WLS in order to control levels of WNT signaling.

KEY WORDS: Neural tube closure, WNT signaling, Wntless, Sorting nexin, Retrograde transport, SNX3

INTRODUCTION

Neural tube (NT) closure is the process by which the embryonic precursor of the mammalian brain and spinal cord is formed. It is a highly dynamic morphogenetic process that starts with the specification of the neural epithelium, which thickens to become the flat neural plate. Molecular signals from the nonneural ectoderm, surrounding mesoderm and ventral notochord, as well as forces generated by cell and tissue movements, enable the flat neuroepithelial plate to intercalate toward the midline and elongate along the anterior-posterior axis as well as form medial and lateral hinge points in the neural plate to 'roll up' and ultimately allow the neural folds to fuse together, forming a closed tube along the length of the rostral-caudal axis (Ray and Niswander, 2012; Wilde et al., 2014; Juriloff and Harris, 2018). This neuroepithelial tube continues to grow and differentiate into the cell types of the brain and spinal cord.

[1]Cell Biology, Stem Cells, and Developmental Biology Graduate Program, University of Colorado Anschutz Medical Campus, Aurora, CO 80045, USA. [2]Department of Molecular, Cellular, and Developmental Biology, University of Colorado Boulder, Boulder, CO 80309, USA. [3]The Jackson Laboratory, Bar Harbor, ME 04609, USA. [4]Department of Pediatrics, McGovern Medical School, University of Texas Health Science Center at Houston, Houston, TX 77030, USA.

*Author of correspondence (lee.niswander@colorado.edu)

K.S.A., 0000-0002-2694-5833; L.A.N., 0000-0002-9959-0594

Handling Editor: Patrick Tam
Received 5 May 2020; Accepted 9 October 2020

Neural tube defects (NTDs) affect 1/1000 live births worldwide, making it the second most common birth defect (Zaganjor et al., 2016). The most common types of NTDs are the cranial NTD exencephaly that ultimately results in anencephaly and the caudal NTD spina bifida or myelomeningocele (Zaganjor et al., 2016). Current treatment options for NTDs are often inefficacious and identifying methods to prevent NTDs have been the main focus of researchers. This led to public health campaigns of folic acid supplementation to reduce the risk for NTDs. However, folic acid supplementation has not eliminated NTDs, indicating our opacity in understanding the full etiology of NTDs and how to prevent them (Au et al., 2010; Wilde et al., 2014). The mouse has been invaluable in defining the genetic contributions to NT closure and, currently, over 200 mutations have been associated with NTDs in mice (a list of genes identified as required for mouse NT closure is available at sbseqconsortium.org/mouse-ntd-model). Cranial NTD is more common in mouse, whereas in the human population caudal NTDs are predominant (Harris and Juriloff, 2007; Au et al., 2010). Despite this discrepancy, investigating NTDs in the mouse model is advantageous to understand the molecular mechanisms of NT closure and genetic data from mouse has greatly informed studies to uncover the etiology of NTDs in humans.

Specifically, genes that facilitate cell-to-cell communication via intracellular signaling pathways are required for neural tube closure through bone morphogenetic protein (BMP) signaling, sonic hedgehog (SHH) signaling and wingless integrated 1 (WNT) signaling (Kanzler et al., 2000; Ybot-Gonzalez et al., 2002; Castranio and Mishina, 2009; Misra and Matise, 2010; Murdoch and Copp, 2010; Zhao et al., 2014; Allache et al., 2015; Anderson et al., 2016). WNT signaling in particular is important for neural patterning, growth, cell intercalation and neural tube closure. WNT signaling acts to induce both the canonical WNT signaling pathway for transcription of WNT target genes, such as *Axin2*, *Lef1* and *Pax3* in the neural epithelium, and the non-canonical WNT signaling pathway for cell intercalation of the neural epithelium and elongation of the body axis in a process called convergent extension (Perry et al., 1995; Carter et al., 2005; Qian et al., 2007; Gao, 2012). Many non-canonical WNTs act through planar cell polarity proteins, such as VANGL2, to initiate cellular polarity changes to induce convergent extension in the neural epithelium (Greene et al., 1998; Juriloff and Harris, 2012). Canonical WNTs bind their co-receptors [frizzled (FZD) proteins and LRP5/6], which inactivates the β-catenin destruction complex to induce WNT target gene expression for maintaining anterior-posterior and dorsal-ventral identity of the neural tube, and for neural tube closure, brain development and craniofacial development (Song et al., 2009; Wang et al., 2010; Zhao et al., 2014). Briefly, WNT signaling is the process by which post-translationally modified proteins called WNTs are secreted from cells to be received by surface receptors of the receiving cell. This results in either the specific transcription of WNT target genes (canonical WNT signaling) or activation of

Development (2020) 147, dev192518. doi:10.1242/dev.192518

Table 1. *Snx3* litters show normal Mendelian ratio and KO embryos show cranial neural tube defects

Genotype	N	% Embryos expected	% Embryos observed	% Embryos with NTD
Wild type (*Snx3*$^{+/+}$)	123	25	22	0
Heterozygous (*Snx3*$^{+/-}$)	320	50	56	0
Knockout (*Snx3*$^{-/-}$)	129	25	22	100

cytoskeletal reorganization (non-canonical WNT signaling) in a spatially and temporally regulated manner to control tissue and organ development (Nusse et al., 1991). WNT signaling is an ancient and conserved signaling system that, when disrupted, is implicated in many developmental disorders (Logan and Nusse, 2004). Both canonical and non-canonical WNT proteins require an indispensable binding protein, Wntless (WLS), in order to be trafficked to the cell surface for proper secretion and signaling to neighboring cells. The role of WLS is evolutionary conserved and in both *C. elegans* and *D. melanogaster*, the trafficking of WLS is dependent on sorting nexin (SNX) proteins (Zhou et al., 2003; Belenkaya et al., 2008; Harterink et al., 2011; Zhang et al., 2011; Yu et al., 2014; Sun et al., 2017; McGough et al., 2018).

Sorting nexins are a class of intracellular trafficking proteins characterized by the presence of the Phox homology domain (PX domain) (Haft et al., 1998; Johannes and Wunder, 2011). The PX domain binds to phospholipid bilayers within the cell such as membranes of endosomes and lysosomes, then binds specific cargo for intracellular transport to carry out specific functions (Worby and Dixon, 2002; Lenoir et al., 2018; Cui et al., 2019). This article investigates the role of *Snx3* for specific transport of the WNT ligand-binding protein WLS to enable NT closure. A specific role for SNX3 in mammalian development has not been studied.

The intracellular trafficking machinery that facilitates cellular signaling during NT closure has been explored in a few cases. For example, SEC24B is a cargo-sorting protein that specifically sorts VANGL2 into COPII-coated vesicles to be trafficked from the endoplasmic reticulum to the Golgi body (Merte et al., 2010; Yang et al., 2013). Mutations in *SEC24B* are present in human cohorts with NTDs, highlighting the importance of this cargo-sorting protein for correct NT closure. Although disruption of intracellular trafficking can disrupt embryonic development, whether specific cargo and specific trafficking events are required for NT closure and development is not fully understood. Thus, understanding the biology of NT closure at the cellular level, as investigated here, is crucial to adopting a prevention-based method of treatment to decrease the risk and incidence of NTDs.

Recently, the Knockout Mouse Phenotyping Program (KOMP2) created a null allele of *Snx3*, a sorting nexin gene that is crucial for intracellular retrograde trafficking and recycling (Haft et al., 1998). *Snx3*$^{-/-}$ KO mice show cranial NTDs, brain and craniofacial deformities, and embryonic lethality (mousephenotype.org/data/genes/MGI:1860188). NTDs are currently not associated with retrograde trafficking defects, which makes it interesting to explore the function of SNX3 in the process of neural tube closure.

Here, we investigate the role of SNX3 in the pathogenesis of NTDs. Our data show that *Snx3*$^{-/-}$ embryos display both neural patterning and convergent-extension defects, suggesting disruption in WNT signaling. Using both *in vivo* and *in vitro* approaches, we show that SNX3 is essential for NT closure via recycling of the WNT ligand-binding protein WLS to promote both canonical and non-canonical WNT signaling. In the absence of SNX3, WLS is targeted for degradation in the lysosome and the level of WNT signaling is reduced. Moreover, we find that a *SNX3* mutation identified in an NTD-affected individual disrupts WLS recycling. Rescue of the NTD phenotype in mouse embryos treated with a WNT agonist further highlights the importance of SNX3-WLS trafficking to maintain a proper balance in WNT signaling during NT closure.

RESULTS

Mice lacking *Snx3* show 100% penetrant neural tube defects and are reduced in size

The KOMP2 program at The Jackson Laboratory generated the Snx3tm1.1(KOMP)Vlcg (MGI:1860188) allele following microinjection of embryonic stem (ES) cells targeted by the Velocigene program at Regeneron Pharmaceuticals as part of the KOMP program (clone 155528-B8). This deletion generated a null allele of *Snx3*. Preliminary studies by the KOMP2 program showed that heterozygous *Snx3*$^{-/+}$ mice are phenotypically normal; however, intercrosses to produce animals for the adult and embryonic phenotyping pipeline (PMID:28650483, PMID:27626380) showed *Snx3*$^{-/-}$ embryos at normal Mendelian ratios with death by birth (Table 1). *Snx3*$^{-/-}$ null embryos displayed multiple severe phenotypes, including cranial NTD. We characterized the NTD phenotype starting at embryonic day 8.5 (E8.5) at the beginning of neurulation, and at E9.5, E10.5 and E15.5 (Fig. 1). Wild-type and mutant embryos were somite matched, and we observed consistent developmental disruptions in the *Snx3*$^{-/-}$ embryos beginning with

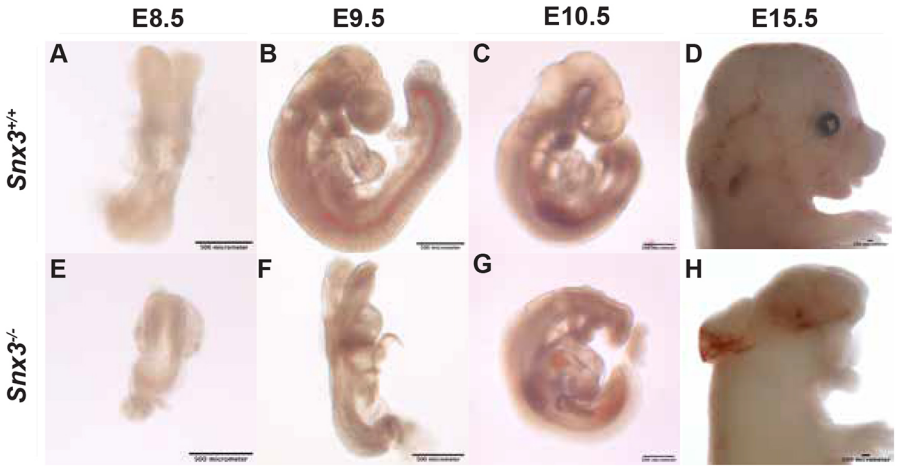

Fig. 1. *Snx3*$^{-/-}$ embryos show cranial neural tube defects and craniofacial defects, and are reduced in size. (A-H) Wild-type (A-D) and *Snx3*$^{-/-}$ (E-H) embryos dissected at E8.5, E9.5, E10.5 and E15.5. *Snx3*$^{-/-}$ mutants show altered cranial morphology and reduced size at all ages, which were somite matched for comparison at E8.5-10.5. *Snx3*$^{-/-}$ embryos at E8.5 (E) are much shorter than somite-matched wild-type littermates; by E9.5 (F) the mutants show an open cranial neural tube defect that persists throughout embryonic development, leading to anencephaly (G,H). A total of 572 embryos were dissected at various ages and their NTD status recorded. Normal Mendelian ratios were observed and 100% of *Snx3*$^{-/-}$ embryos displayed NTD (Table 1). Scale bars: 500 µm.

Development (2020) 147, dev192518. doi:10.1242/dev.192518

E8.5. Although the *Snx3* KO embryos were much shorter than the wild-type littermates, they were not developmentally delayed and somite number did not vary significantly within a litter. At E9.5 and E10.5, 100% of *Snx3*$^{-/-}$ embryos exhibited cranial NTD, ultimately leading to anencephaly with the brain tissue exposed at E15.5 (n=129 *Snx3* mutants observed). At all stages, *Snx3*$^{-/-}$ embryos were reduced in size compared with somite-matched wild type (Fig. 1). All *Snx3*$^{-/-}$ embryos also show severe craniofacial defects. Staining of E9.5 and E12.5 heterozygous embryos to detect LacZ driven by *Snx3* regulatory elements showed strongest expression at E9.5 in the neural epithelium, craniofacial region and heart (Fig. S1A,C,D), with ubiquitous expression at E12.5 (Fig. S1B). In terms of neurulation, only cranial NTD is observed: the reason for this restricted phenotype is unclear, as LacZ expression was detected in the neural epithelium along the rostral-caudal axis. This could reflect a more-complex morphogenesis of the cranial neural folds or perhaps alternative pathways that can compensate for *Snx3* loss during spinal neural tube closure. These data indicate that *Snx3* is crucial for cranial neural tube closure and embryonic development in mice.

Snx3$^{-/-}$ embryos show disrupted expression of canonical WNT target genes and convergent-extension defects similar to disruption of non-canonical WNT signaling

The shortened length of *Snx3*$^{-/-}$ embryos resembled mice with mutations that disrupt the non-canonical WNT planar cell polarity pathway (Ikeya et al., 1997; Wang, 2006; Qian et al., 2007). This led us to ask whether WNT signaling was disrupted in *Snx3*$^{-/-}$ embryos. To address this issue, we first performed RNA *in situ* hybridization to assess the expression of common canonical WNT target genes, *Axin2*, *Lef1* and *Pax3*. These genes are expressed in the anterior cranial neural folds of E8.5 wild-type embryos (Fig. 2A,B, E,F,I,J). However, in the somite-matched *Snx3*$^{-/-}$ E8.5 whole embryos, expression of *Axin2*, *Lef1* and *Pax3* was greatly decreased in the anterior cranial neural folds (Fig. 2C,D,G,H,K,L). Furthermore, we used a TCF/Lef:H2B-GFP transgenic reporter mouse to visualize WNT signaling activity in the cranial neural folds and observed a significant decrease in GFP in the neural epithelium of *Snx3*$^{-/-}$ embryos compared with their somite-matched wild-type littermates (Fig. 2M-P, Fig. S2A-C). These data together indicate an overall significant decrease in WNT signaling and target canonical WNT gene expression in the cranial neural folds of *Snx3*$^{-/-}$ embryos, including expression of *Pax3*, which is required for NT closure (Zhao et al., 2014).

There was also a striking difference in the overall shape of the E8.5 *Snx3*$^{-/-}$ embryos compared with wild type. The *Snx3*$^{-/-}$ embryos appeared much shorter and wider than their somite-matched wild-type littermates. This phenotype is similar to a disruption in non-canonical WNT signaling (planar cell polarity), which leads to defective convergent extension of the neural epithelium and NTDs. A quantitative assessment for a convergent extension defect at early embryonic stages is to calculate the length-to-width ratio of the mouse embryo (Ybot-Gonzalez et al., 2007). Therefore, we quantified length-to-width ratios on all somite-matched wild-type and *Snx3*$^{-/-}$ E8.5 embryos and found a statistically significant smaller length-to-width ratio of *Snx3*$^{-/-}$ compared with wild-type embryos (Fig. 3). Taken together, the lack of expression of canonical WNT target genes *Axin2*, *Lef1* and *Pax3*, decreased GFP expression using the TCF/Lef:H2B-GFP transgenic reporter, and the decreased length-to-width ratio in the *Snx3*$^{-/-}$ embryos indicate that both canonical WNT signaling and non-canonical WNT signaling are disrupted in embryos that lack *Snx3* function.

Snx3$^{-/-}$ embryos have defects in secretion of both canonical and non-canonical WNTs

As *Snx3* mutant embryos display the hallmarks of disrupted canonical and non-canonical WNT signaling, we next asked whether loss of *Snx3* results in reduced WNT protein secretion. To test this, we compared wild-type and *Snx3*$^{-/-}$ mouse embryonic fibroblasts (MEFs) using enzyme-linked immunosorbent assays (ELISA) with cell culture media collected from identically seeded and processed in parallel wild-type or *Snx3*$^{-/-}$ MEFs transfected with canonical *Wnt1* or non-canonical *Wnt5a* expression constructs. This showed lower WNT1 and WNT5A protein secretion into the media from the *Snx3*$^{-/-}$ cells compared with wild type (Fig. 4). To directly test that the secretion defect was solely due to the lack of *Snx3,* we added a plasmid encoding wild-type SNX3 to the *Snx3*$^{-/-}$ cells. This showed a restoration of WNT1 and WNT5A secretion into the media (Fig. 4), indicating the importance of SNX3 in maintaining proper levels of WNT secretion. These data indicate a defect in secretion of both canonical and non-canonical WNTs in the absence of *Snx3* and aligns with our *in vivo* results.

SNX3 traffics WLS and is required for correct recycling of WLS within the cell

The data presented so far provide evidence that *Snx3* is important for NT closure via a role in regulation of canonical and non-canonical WNT signaling. The mechanism of action of the SNX3 homolog in *C. elegans* and *D. melanogaster* is in the intracellular retrograde trafficking of WLS, the WNT ligand binding protein (Harterink et al., 2011; Zhang et al., 2011; McGough et al., 2018). In these contexts, SNX3 transports the endocytosed ligand-free WLS from the early endosome of the cell to the trans-Golgi network, where WLS binds WNT to facilitate the process of normal WNT secretion (Johannes and Wunder, 2011). Without SNX3, WNT secretion decreases in both *C. elegans* and *D. melanogaster* (Belenkaya et al., 2008; Harterink et al., 2011; Johannes and Wunder, 2011; Zhang et al., 2011). To determine whether SNX3 assumes a similar role in trafficking WLS in mammals, we evaluated the colocalization and relationship between WLS and SNX3. We performed live cell imaging of wild-type MEFs transfected with plasmids to express SNX3-GFP and WLS-RFP fusion proteins. This showed that SNX3 colocalizes with WLS in mouse cells (Fig. 5A-B). Furthermore, SNX3 and WLS traffic together in real time. Trafficking of SNX3-GFP and WLS-RFP was captured over 10 s intervals, showing both proteins budded off the SNX3-GFP labeled early endosome together (Fig. 5C). In the wild-type setting we would predict WLS to localize with the early endosome for recycling, rather than being trafficked to the lysosome. In the absence of SNX3, we hypothesized that WLS would be mis-trafficked to the lysosomal pathway for degradation, thus disrupting the recycling of WLS and leading to dysregulation of the tightly regulated WNT secretion cycle. To test whether the lack of SNX3 results in WLS being mis-trafficked to the lysosome, plasmids coding for fusion proteins to tag the early endosome (RAB5-BFP) or the lysosome (LAMP1-GFP), as well as WLS-RFP, were transfected into wild-type and *Snx3*$^{-/-}$ cells. We then calculated the colocalization of WLS with the early endosome or the lysosome. We observed that WLS predominantly colocalizes with the early endosome in wild-type cells, whereas WLS predominantly colocalizes with the lysosome in *Snx3*$^{-/-}$ cells (Fig. 5D-G″,J,J′,K,K′,M). To confirm that this mis-sorting of WLS to the lysosome was due to the absence of SNX3, we introduced exogenous SNX3 into *Snx3*$^{-/-}$ cells and saw that the localization of WLS was restored to the early endosome (Fig. 5H-I, L,L′,M). Higher magnification of the endosomes (RAB5-BFP

Development (2020) 147, dev192518. doi:10.1242/dev.192518

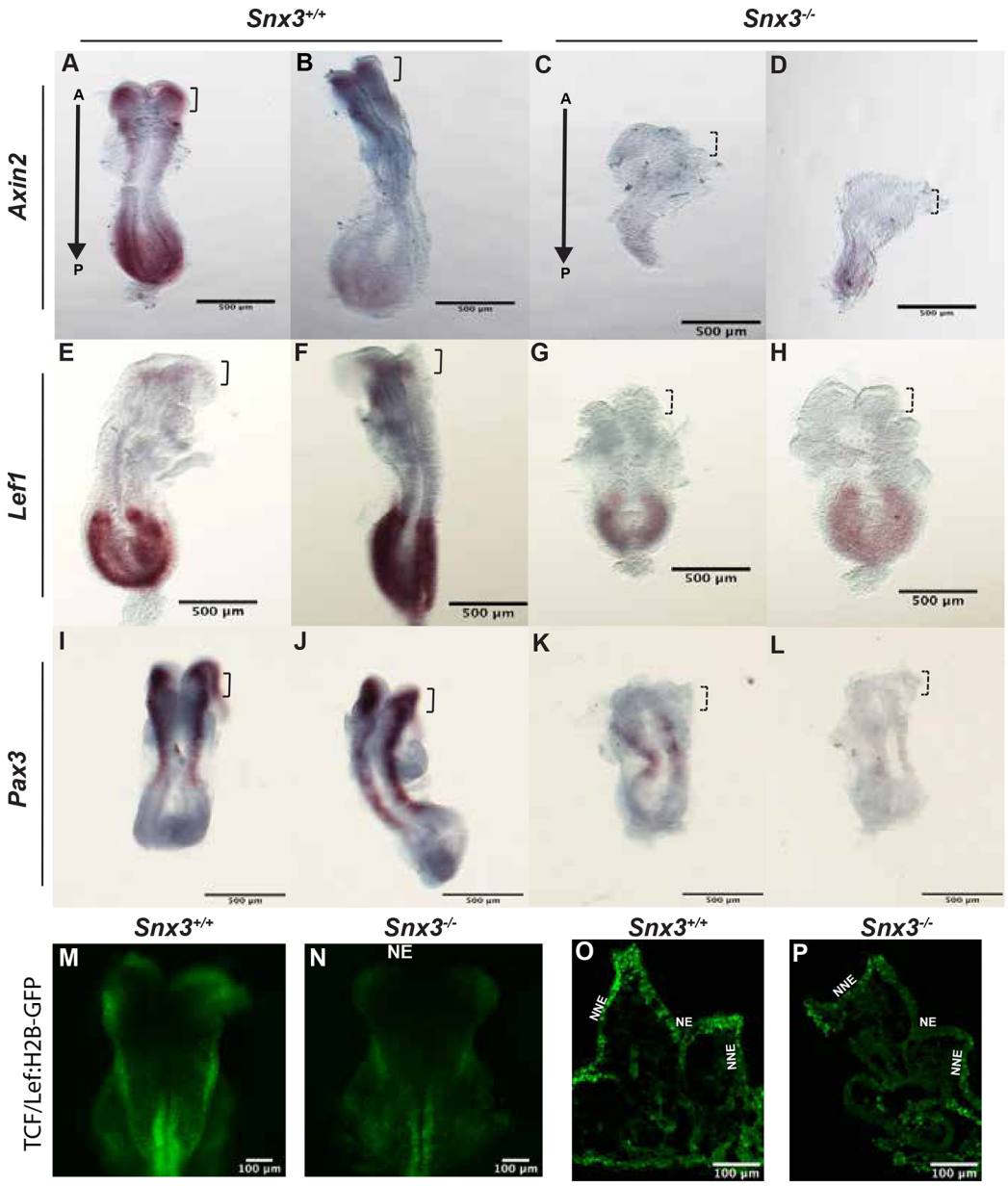

Fig. 2. *Snx3*$^{-/-}$ embryos show decreased expression of downstream canonical WNT target genes in the cranial neural folds. (A,B,E,F,I,J) Wild-type embryos at E8.5 show expression of *Axin2* (A,B), *Lef1* (E,F) and *Pax3* (I,J) in the cranial neural folds (brackets). (C,D,G,H,K,L) In contrast, *Snx3*$^{-/-}$ embryos at E8.5 show decreased expression of *Axin2* (C,D), *Lef1* (G,H) and *Pax3* (K,L) in the cranial neural folds (dashed brackets). *n*=2 for each genotype for each gene tested. Anterior (A) is at the top and posterior (P) at the bottom of each panel. (M-P) TCF/Lef:H2B/GFP reporter whole-mount (M,N) and then sectioned (O,P) embryos were used to visualize Wnt/β-catenin activity of wild-type and *Snx3*$^{-/-}$ embryos at E8.5. *Snx3*$^{-/-}$ embryos showed significant decrease in GFP fluorescence, indicating less Wnt/β-catenin activity in particular in the neural epithelium (NE), with no obvious effect on non-neural ectoderm (NNE) activity. Scale bars: 500 µm in A-L; 100 µm in M-P.

labeled) and lysosomes (LAMP1-BFP) showed that WLS predominantly colocalizes to the early endosome in wild-type cells, the lysosome in *Snx3*$^{-/-}$ cells, and endosome localization is rescued in *Snx3*$^{-/-}$ cells transfected with exogenous *Snx3* plasmid (Fig. 5J-L′).

SNX3 specifically localizes and binds to phosphatidyl inositol-3-phosphate (PI3P) predominantly at early endosomal membranes (Lenoir et al., 2018). The early endosome is the site of protein sorting for recycling either to the plasma membrane or trans-Golgi network, or for lysosomal degradation (Delevoye et al., 2014; Cullen and Steinberg, 2018; Wang et al., 2018; Singla et al., 2019). Thus, if lack of *Snx3* results in WLS being mis-sorted to the lysosome followed by lysosomal degradation, we would predict to observe less WLS-RFP in the cells lacking *Snx3*. Consistent with this hypothesis, our live-cell imaging data show a reduced level of WLS-RFP protein in *Snx3*$^{-/-}$ cells compared with wild-type cells (Figs 5D,E,F,G and 6A,B,E). To evaluate further whether WLS is being degraded without *Snx3*, we treated the cells with bafilomycin, a lysosomal degradation inhibitor. Quantification of WLS in wild-type and *Snx3*$^{-/-}$ cells treated with bafilomycin showed an increase in the WLS levels when lysosomal degradation was inhibited (Fig. 6C-E). There was a small, but not significant, increase in the treated wild-type cells compared with untreated wild-type cells (Fig. 6C-C′,E), consistent with the idea that this recycling pathway

Development (2020) 147, dev192518. doi:10.1242/dev.192518

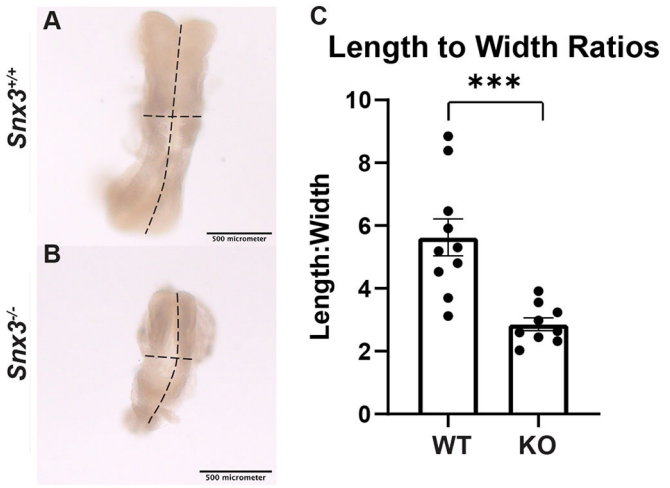

Fig. 3. *Snx3*$^{-/-}$ embryos show a significant change in length-to-width ratio compared with their wild-type littermates, indicating a defect in convergent extension. (A,B) Wild-type (n=10) and *Snx3*$^{-/-}$ (n=9) E8.5 embryos were dissected and their length and width measured in µm using Image J. A and B represent an example of these measurements. (C) Length was divided by width and plotted as a ratio. Images in A and B are the same images as in Fig. 1 A,E. A two tailed t-test was performed to test statistical significance. Error bars represent s.e.m., ***P<0.001. Scale bars: 500 µm.

is in a steady state of retrograde trafficking regulation from the early endosome to the trans-Golgi or the lysosome. In the *Snx3*$^{-/-}$ cells, we observed a striking increase in WLS levels in the bafilomycin-treated group compared with the untreated group, and the WLS-RFP was largely in LAMP1-positive lysosomal vesicles (Fig. 6D-E). Furthermore, we observed statistically similar WLS levels in bafilomycin-treated *Snx3*$^{-/-}$ cells as in both treated and untreated wild-type cells (Fig. 6E). This indicates that the WLS levels are restored to wild-type levels when lysosomal degradation is halted. Taken together, these data are consistent with the defective recycling of WLS in *Snx3*-deficient cells and suggest that SNX3 is crucial in the trafficking of WLS from the early endosome for recycling in order to bind another WNT protein and facilitate another cycle of WNT secretion. Furthermore, in the absence of SNX3, WLS is trafficked to the lysosome for degradation, thus reducing WNT signaling on a cellular level.

The *SNX3* mutation identified in a NTD-affected individual results in functionally impaired SNX3 protein

The protein sequence of SNX3 is 100% conserved from mice to humans (NP_059500.2 and NP_00376.1). This and the strong NTD phenotype in mice led to the question of whether sequence variation in the *SNX3* gene may genetically contribute to NTDs in humans. Whole-exome sequencing of a cohort of 511 myelomeningocele-affected sporadic individuals identified a missense point mutation (GRCh37/hg19; 6:108582021:G:T) in the *SNX3* gene in one individual with a NTD. Specifically, the subject is heterozygous for the *SNX3 p.Asn35Lys* variant. The overall dataset cannot be released due to HIPAA Privacy Rules; however, the subject exhibited myelomeningocele and was heterozygous for the *SNX3* variant as well as another heterozygous variant in the *CITED2* gene (chr6:139695005:T:C; p.His31Arg), which is also associated with NTD. The *SNX3 p.Asn35Lys* variant in this subject resulted in a G-to-T transversion in exon 1 (ORF pos. 105), creating an asparagine-to-lysine amino acid change (Fig. 7A). This is a novel point mutation that has not been reported in the literature or public variant databases. The Combined Annotation Dependent Depletion (CADD) score for this point mutation is 25.8, predicting the change to be deleterious to SNX3 function. To test whether this specific point mutation results in a functionally impaired SNX3, we performed site-directed mutagenesis to generate *SNX3-p.Asn35Lys-GFP* mutant plasmid, then transfected it into *Snx3*$^{-/-}$ MEFs along with *Wls-RFP*. Colocalization analysis indicated that there was significantly less SNX3-p.Asn35Lys-GFP colocalized with WLS-RFP compared with wild-type SNX3 (Fig. 7B-D). Furthermore, our live-cell imaging showed reduced WLS fluorescence, consistent with our results above that loss of SNX3 function results in aberrant trafficking to the lysosome and degradation (Fig. 7D′). Thus, we treated the *SNX3-p.Asn35Lys-GFP* cells with the lysosomal inhibitor bafilomycin to determine whether WLS was being degraded in the context of the human mutation. We observed that WLS fluorescence was significantly increased upon treatment with bafilomycin in the *SNX3-p.Asn35Lys-GFP* cells compared with the untreated *SNX3-p.Asn35Lys-GFP* cells (Fig. 7E,F). These data indicate that this novel genetic variant identified in an NTD-affected individual could functionally impair SNX3 protein and result in WLS degradation and reduced WNT signaling.

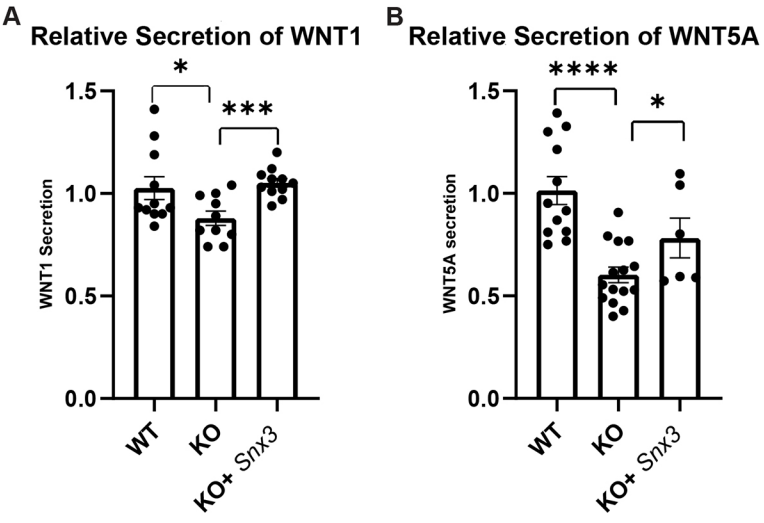

Fig. 4. *Snx3*$^{-/-}$ cells secrete less WNT1 and WNT5A compared with wild-type cells, indicating a defect in both canonical and noncanonical WNT secretion. (A,B) Wild-type or *Snx3*$^{-/-}$ cells were transfected with either *Wnt1* (A), which is considered a canonical WNT, or *Wnt5a* (B), which is considered a non-canonical WNT. The culture media were collected and the absorbance measured by ELISA. Experimental conditions were normalized to wild type. (A) The relative secretion of WNT1 is reduced in *Snx3*$^{-/-}$ cells, relative to wild-type cells, and the secretion defect can be rescued by transfection of a plasmid containing normal *Snx3* into *Snx3*$^{-/-}$ cells. (B) The relative secretion of WNT5A is reduced in *Snx3*$^{-/-}$ cells, relative to wild-type cells, and the secretion defect can be rescued by transfection of a plasmid containing normal *Snx3* into *Snx3*$^{-/-}$ cells. All experiments were carried out in parallel with identical numbers of cells seeded and plasmid transfected. The number of biological and technical replicates are indicated in the Materials and Methods section. A two-tailed t-test was performed to test for statistical significance. Error bars represent s.e.m., ****P<0.0001, ***P<0.001, *P<0.05.

Development (2020) 147, dev192518. doi:10.1242/dev.192518

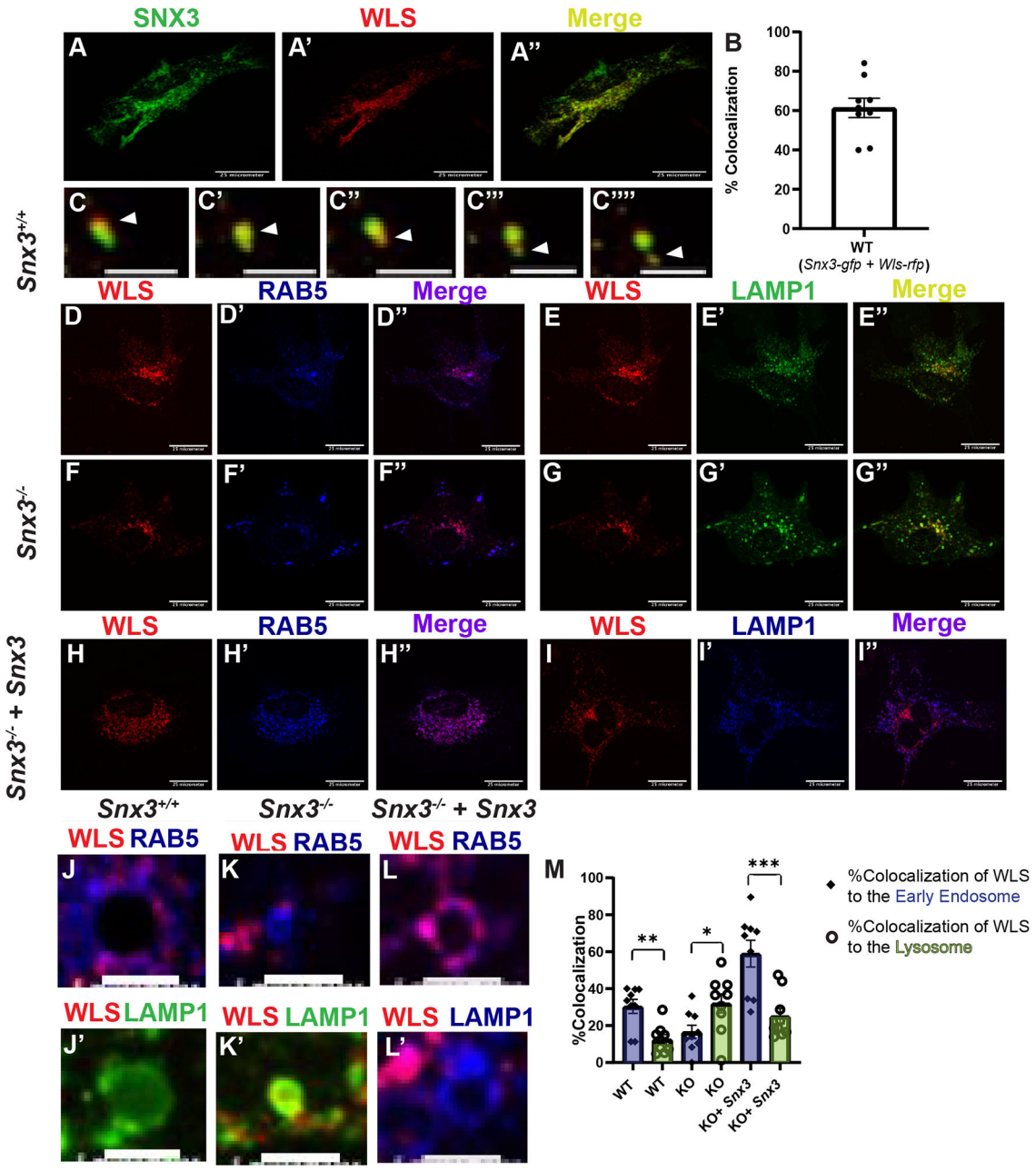

Fig. 5. SNX3 and WLS colocalize and traffic together to the early endosome in wild-type cells, whereas loss of SNX3 results in trafficking of WLS to the lysosome. (A-B) *Snx3* wild-type mouse embryonic fibroblasts transfected with *Snx3-GFP* and *Wls-RFP* show significant colocalization. (C-C″″) SNX3 traffics with WLS in wild-type cells. Arrowheads indicate colocalization of SNX3-GFP and WLS-RFP as these two proteins bud off from an endosome in wild-type cells (time interval between each panel is 10 s). (D-E″,J,J′) In wild-type cells, WLS-RFP predominantly colocalizes with RAB5-BFP, a marker of the early endosome (D-D″,J) and not with LAMP1-GFP, a marker of the lysosome (E-E″,J′) (**P<0.01). (F-G″,K,K′) In $Snx3^{-/-}$ cells, WLS-RFP predominantly colocalizes with the lysosomal marker LAMP1-GFP (G-G″,K′) instead of early endosome RAB5-BFP (F-F″,K) (*P<0.05). (H-I″,L,L′) Transfection of $Snx3^{-/-}$ cells with exogenous wild-type*Snx3-gfp* restores WLS-RFP to predominant colocalization with RAB5-BFP in the early endosome (H-H″,L), and greatly reduces colocalization with LAMP1-BFP (I-I″,L′) (***P<0.001). (J-L′) Higher magnification of individual RAB5-BFP early endosome vesicle and LAMP1-GFP lysosome vesicle with WLS localization. (M) Graph represents the mean colocalization of WLS-RFP/RAB5-BFP and WLS-RFP/LAMP1-GFP in wild-type cells, in $Snx3^{-/-}$ cells and in $Snx3^{-/-}$ cells rescued with *Snx3-gfp*. For all experiments, n=3 biological replicates and 3 technical replicates; more than nine cells were observed. Error bars represent s.e.m. Two tailed t-tests were performed to test for significance. *P<0.05, **P<0.01, ***P<0.001. Scale bars: 25 µm A-A″,D-I″; 5 µm in C-C″″,J-L′. All images show individual cells or vesicles.

Snx3 KO embryos can be rescued with lithium chloride treatment

Our data show that the absence of *Snx3* results in disrupted WLS recycling and reduced WNT secretion and signaling, and leads to NTD in mice. This suggests that it may be possible to rescue the NTD in the $Snx3^{-/-}$ mice by pharmacologically stimulating the WNT signaling pathway downstream of WNT reception. To do so, we used lithium chloride (LiCl), which inhibits the phosphorylation and degradation of β-catenin, allowing β-catenin to translocate to the nucleus and bind TCF/LEF transcription factors to induce WNT target gene expression, in the absence of WNT signaling (Klein and Melton, 1996). As LiCl stimulates the canonical WNT signaling

Development (2020) 147, dev192518. doi:10.1242/dev.192518

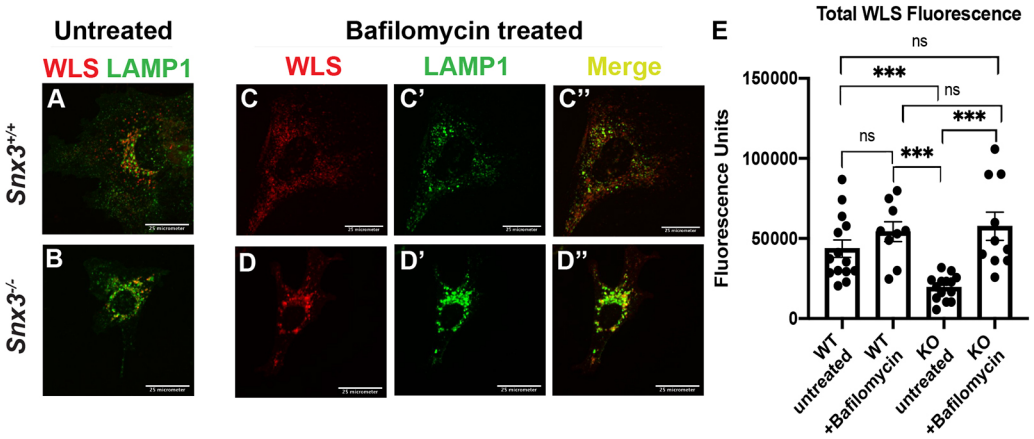

Fig. 6. WLS levels are reduced via lysosomal degradation in *Snx3*$^{-/-}$ cells, and WLS levels are restored when lysosomal degradation is pharmacologically inhibited. (A,B,E) In untreated cells, *Snx3*$^{-/-}$ cells show decreased WLS-RFP overall (B,E) relative to wild-type cells (A,E). (C-C″) Wild-type cells treated with 100 nm bafilomycin for 3 h to stop lysosomal degradation show WLS fluorescence throughout the cytoplasm, including LAMP1-positive lysosomes. (D-D″) *Snx3*$^{-/-}$ cells treated with bafilomycin show a statistically significant increase in WLS fluorescence, and much of the WLS is seen in LAMP1-positive lysosomes. (E) Graph comparing WLS fluorescence in wild-type untreated cells and wild-type bafilomycin-treated cells (ns), *Snx3*$^{-/-}$ untreated cells and *Snx3*$^{-/-}$ bafilomycin-treated cells (***P<0.001), wild-type bafilomycin-treated cells and *Snx3*$^{-/-}$ untreated cells (***P<0.001), wild-type bafilomycin-treated cells and *Snx3*$^{-/-}$ bafilomycin-treated cells (ns), wild-type untreated cells and *Snx3*$^{-/-}$ untreated cells (***P<0.001), and wild-type untreated cells and *Snx3*$^{-/-}$ bafilomycin-treated cells (ns). For all experiments, n=3 biological replicates with at least three technical replicates. Error bars represent s.e.m. Two-tailed t-tests were performed to test for statistical significance. Scale bars: 25 µm.

pathway, we predicted that the NTD would be only partially rescued. However, as the canonical and non-canonical WNT signaling pathways frequently overlap and interact, it is possible that both canonical and non-canonical WNT signaling may be stimulated by LiCl (Komiya and Habas, 2008). Thus, we used a LiCl treatment regime similar to others (Wang et al., 2010) in which pregnant dams received intraperitoneal injections of 300 µl of LiCl on E7.5 and E8.5, and embryos were dissected at E10.5. These injection time points were chosen to stimulate the WNT pathway at the time of neural induction and at the start of cranial neurulation. LiCl treatment did not affect wild-type embryos (Fig. 8A, Fig. S3A-C) but strikingly rescued the NTD in 50% of the *Snx3*$^{-/-}$ embryos dissected (Fig. 8B, Fig. S3D-F). The other 50% of the *Snx3*$^{-/-}$ embryos dissected from these litters with LiCl treatment still showed cranial NTD (Fig. 8C, Fig. S3G-I). These data indicate that SNX3 is crucial for NT closure and that the key function of SNX3 at this time of development is in the regulation of WNT signaling.

DISCUSSION

Here, we show that SNX3 is crucial for mammalian neural tube closure. SNX3 functions to recycle the WNT ligand-binding protein WLS to regulate and facilitate additional cycles of canonical WNT secretion for the expression of downstream WNT target genes, as well as non-canonical WNT secretion for convergent extension in the neural epithelium for NT closure. In the absence of SNX3, WLS is mis-trafficked to the lysosomal pathway and is degraded, disrupting the tight regulation of WNT secretion. Furthermore, we show that the NTD can be fully rescued in 50% of *Snx3*$^{-/-}$ embryos by pharmacologically stimulating the WNT signaling pathway. Our studies demonstrate that intracellular trafficking of WLS via SNX3 is essential to maintain proper levels of WNT signaling during mammalian development.

Snx3$^{-/-}$ embryos show 100% penetrant cranial NTD, explored here, as well as brain and craniofacial phenotypes, reduced size, and embryonic lethality. However, as we have shown that the NTD phenotype is due to reduced WNT signaling, it is curious that embryonic development is not more extensively disrupted given the fact that WNT signaling is important for so many aspects. A complete knockout of *Wls* in the mouse results in embryonic lethality at gastrulation because it stops all WNT secretion (Fu et al., 2011). It is important to note that SNX3 regulates WLS recycling. As WLS and WNT are still present and able to interact for at least one round of secretion and signaling, loss of SNX3 would not abolish WNT signaling, as in the *Wls* KO, but would be expected to decrease the overall level of WNT signaling. Moreover, at the time of neurulation, Snx3 is predominantly expressed in the neural epithelium and craniofacial tissues. These data indicate that SNX3 is crucial for some aspects of WLS function but in other tissues *Snx3* is not essential or is perhaps compensated for by another SNX protein, as there are 25 mammalian sorting nexins, each with specific cargo they traffic and a specific cellular localization (Worby and Dixon, 2002). Relative to NT closure, it is possible that the cranial region of the embryo requires higher levels of WNT signaling facilitated by *Snx3* to produce specific developmental outcomes, whereas the caudal region of the embryo might use lower levels of WNT or is better able to compensate for the decrease in WNT regardless of the lack of *Snx3*, perhaps by simply upregulating *Wls*. Furthermore, WNTs are tightly spatially and temporally regulated, and it is possible that the cranial region of the embryo at the early developmental time points is particularly sensitive to alterations in WNT signaling compared with the caudal region of the embryo. Additionally, SNX3 in the context of non-canonical WNT signaling in particular has not been previously reported. The *Snx3*$^{-/-}$ phenotype has provided a new viewpoint into WLS function during NT closure.

The tyrosine residues in the PX domain of SNX3 serve to localize SNX3 to the early endosome through binding of the glycerol moiety in PI3P, which is enriched at the early endosomal membrane (Xu et al., 2001; Lucas et al., 2016). WLS binds the retromer subunit VPS26, which, in turn, is bound to SNX3 through the N-terminal tail of VPS26 (Lucas et al., 2016). SNX3 undergoes conformational changes upon binding the retromer complex (VPS26-VPS35-VPS29) that then allows binding of cargo such as WLS to the retromer complex (Lucas et al., 2016). Given the fact that SNX3

Development (2020) 147, dev192518. doi:10.1242/dev.192518

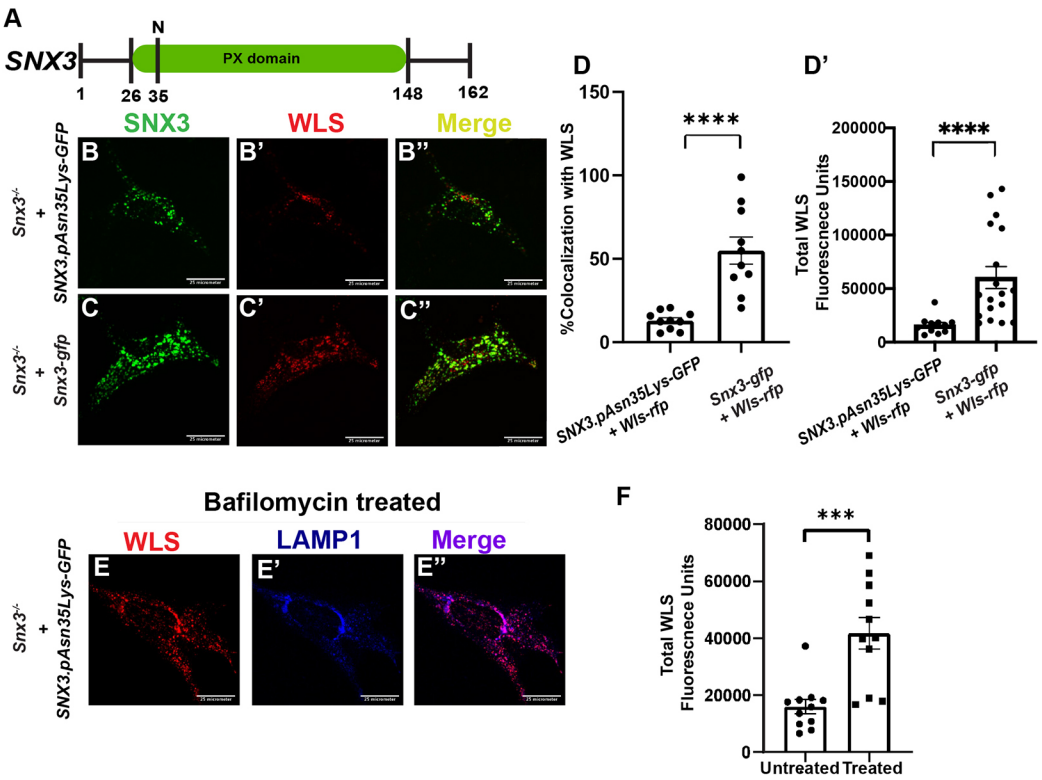

Fig. 7. *SNX3-p.Asn35Lys* results in a functionally impaired protein that does not colocalize with WLS and results in WLS degradation. (A) Schematic of SNX3 and the asparagine at position 35 within the PX domain that is changed to lysine (N35K), as identified in an individual with NTD. (B-D′) A plasmid expressing either SNX3-p.Asn35Lys-GFP or WT SNX3-GFP was transfected along with a plasmid expressing WLS-RFP into *Snx3*$^{-/-}$ cells. (D) There is significantly less colocalization of mutant SNX3 with WLS compared with wild-type SNX3 with WLS (****P<0.0001). (D′) Total WLS fluorescence plotted with statistical analysis to show how levels of WLS compared between the *Snx3* with the human mutation and *Snx3*$^{-/-}$ cells rescued with wild-type plasmid (****P<0.0001). (E-F) Significantly less WLS was observed in *SNX3-p.Asn35Lys-GFP* cells compared with *SNX3-p.Asn35Lys-GFP* cells treated with 100 nm bafilomycin to inhibit lysosomal degradation (***P<0.001). Scale bars: 25 µm. n=3 biological replicates each with at least three technical replicates. Graphs represent three independent experiments. Error bars represent s.e.m. Two-tailed t-tests were performed to test for significance. Scale bars: 25 µm.

undergoes conformational changes based on its binding partners, we hypothesize that the asparagine to lysine amino acid mutation at position 35 in the PX domain of the human protein affects SNX3 conformation and disrupts WLS binding to the retromer subunit VPS26. We show the *SNX3* p.Asn35Lys mutation results in disrupted colocalization with WLS, such that WLS is mis-trafficked to the lysosome, similar to what we observed in *Snx3* loss-of-function MEFs, instead of the normal recycling of WLS back to the trans-Golgi network for further binding of WNT. Loss of *Snx3* in mouse cells and the patient *SNX3* p.Asn35Lys allele both lead to abnormal WLS degradation. In mice, we show that loss of *Snx3* results in decreased WNT signaling during neurulation and leads to NTD. Thus, the *SNX3* p.Asn35Lys mutation could contribute to the NTD phenotype in humans. Furthermore, asparagine at position 35 is a weak nucleophile and would not be expected to be post translationally modified, whereas the point mutation introduces a lysine, which often can be post-translationally modified. Possible post-translational modifications that could be added to the lysine may affect the conformation of SNX3 and also decrease its functionality. Further studies are needed to understand how this point mutation affects the function of SNX3 and distribution of WLS; however, these data provide further evidence to support our hypothesis that *Snx3* is crucial for mammalian neural tube closure because of its colocalization and trafficking roles with WLS.

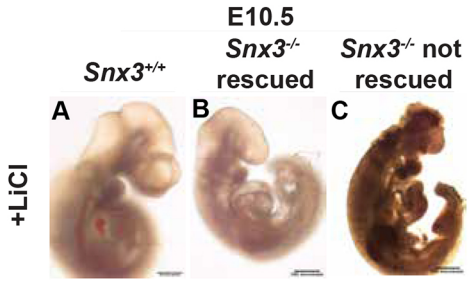

Fig. 8. NTDs in *Snx3*$^{-/-}$ embryos can be rescued with LiCl. (A) E10.5 wild-type embryo from pregnant females intraperitoneally injected with LiCl at E7.5 and E8.5 shows normal neural tube closure. (B) E10.5 *Snx3*$^{-/-}$ embryo from pregnant females intraperitoneally injected with LiCl at E7.5 and E8.5 has closed the neural tube, indicating a full rescue of the cranial NTD. (C) E10.5 *Snx3*$^{-/-}$ embryo in which the NTD was not rescued with LiCl treatment. Embryos are from three independent litters. Wild type, n=6; KO n=8 (of which four showed a fully closed neural tube; P<0.05, Fisher's exact test). Additional embryo photos can be found in Fig. S1. Scale bars: 500 µm.

The fact that the NTD in *Snx3*$^{-/-}$ embryos can be rescued with LiCl shows that WNT is the key mechanistic link between SNX3 and neural tube closure in the mouse model. It is important to note, however, that the NTD was not rescued in all *Snx3*$^{-/-}$ embryos by LiCl treatment. This could suggest the importance of the timing and dosage of treatment, given the gradients of WNT as a morphogen, resulting in rescue rates that differ among litters. In addition, the varying rescue rates could be reflective of the inability to

Development (2020) 147, dev192518. doi:10.1242/dev.192518

sufficiently rescue non-canonical WNT signaling required for NT closure. Alternatively, it is likely that there are other factors involved in NT closure that SNX3 regulates apart from WNT. As trafficking proteins rarely traffic only one cargo, it is possible that there are other factors involved in the NT closure process that are disrupted in the absence of *Snx3*. For example, in erythroid cells, SNX3 also traffics the transferrin receptor (TFRC), which is needed for iron import (Chen et al., 2013). Furthermore, epidemiological studies and studies in mouse models indicate that iron is a crucial micronutrient for embryonic development and neural tube closure (Milunsky et al., 1989; Zohn et al., 2007; Stokes et al., 2016; Li et al., 2018). Perhaps the $Snx3^{-/-}$ NTD phenotype could be rescued more effectively with combined WNT stimulation and iron supplementation.

Overall, we have discovered a previously unreported mechanism by which NT closure is regulated in the mammalian model. The *SNX3* p.Asn35Lys mutation significantly affects SNX3 function and, although this was a heterozygous mutation in the NTD-affected individual, the exquisite sensitivity of NT closure to the levels of WNT signaling suggest this could be a contributing factor to NTD risk. Further studies are required to understand the full role of SNX3 in NT closure and the genetic intersection between *Snx3* and other genes that contribute to this.

MATERIALS AND METHODS

Mouse lines and colony maintenance

All mouse work was carried out in accordance with University of Colorado Boulder Institutional Animal Care and Use Committee (IACUC) policies and procedures, and animals were maintained under standard light and ambient conditions. The genetic background of all mice was C57BL/6J. One male $Snx3^{-/+}$ and one female $Snx3^{-/+}$ mouse was obtained from the KOMP2 program at The Jackson Laboratory, which generated the Snx3tm1.1(KOMP)Vlcg (MGI:1860188) allele following microinjection of embryonic stem (ES) cells targeted by the Velocigene program at Regeneron Pharmaceuticals as part of the KOMP program (clone 155528-B8). Following germline transmission of the targeted allele, the mice were bred to a B6N congenic Sox2-cre line [$Edil3^{Tg(Sox2-cre)1Amc}$/J; JAX STOCK# 14094] to remove the neo selection cassette. The allele consists of 32,453 bp deletion in the *Snx3* gene, replaced by a LacZ cassette, resulting in a complete knockout [allele is B6N(Cg)-$Snx3^{tm1.1(KOMP)Vlcg}$/J, MGI ID is MGI:1860188]. The colony was expanded by crossing littermates and heterozygous males and females were used to generate $Snx3^{-/-}$ (KO) embryos. Vaginal plugs were checked in the morning for timed mating, with noon on the day of positive identification of a plug considered to be embryonic day 0.5. Genotyping was performed using a tail clip or yolk sac digested in lysis buffer and proteinase K overnight at 56°C, and heat inactivated for 10 min at 95°C. Samples were diluted 2:100 and combined with DMSO (New England Biosciences), Amplitaq Gold (ThermoFisher Scientific, N8080241), PCR6 buffer, and forward and reverse primers (IDT) for wild-type or *Snx3* KO, and run on the thermal cycler program 95°C for 5 min followed by 35 cycles of 95°C for 30 s, 60°C for 30 s and 72°C for 1.5 min, the 72°C for 5 min. Samples were run on a 1.5% agarose gel and imaged on the Bio-Rad gel imager system. Bands at 359 base pairs indicated wild type, bands at 576 bp indicated KO, and the presence of both bands indicated heterozygous genotype. Primers were as follows: wild-type *Snx3* forward primer sequence, 5′-TTG GTC TCT TGT CCC ACC TT-3′; wild-type *Snx3* reverse primer sequence: 5′-CTG TAG AGG ACC TGG GTT CG-3′; *Snx3* KO forward primer sequence: 5′-TGT CAA CTG CCA AGA CAA GC-3′; and *Snx3* KO reverse primer sequence: 5′-CGG TCG CTA CCA TTA CCA GT-3′.

Mouse dissections and whole-embryo imaging

Dissections were carried out according to NIH guidelines and IACUC protocol at various time points. To observe the $Snx3^{-/-}$ phenotype, heterozygous parents were crossed and embryos were dissected at E8.5, E9.5, E10.5 and E15.5, and fixed in 4% paraformaldehyde (PFA) at 4°C overnight then washed in 1× phosphate-buffered saline (PBS Thermo Fisher, 10010049). Embryos were imaged on the Olympus IX83 Fluorescence Microscope with a 4× objective (Figs 1 and 7) or the Nikon SMZ18 Stereoscope with Nikon DS-Ri1 CCD-cooled camera with a 3× objective (Fig. 2) and analyzed using Image J.

RNA *in situ* hybridization

Embryos were dissected at E8.5, and embryo phenotypes were recorded at the time of dissection while within the yolk sac, ensuring no mechanical forces affected the shape of the embryos apart from the *Snx3*-related phenotype. Embryos were fixed in 4% PFA prior to processing for whole-mount *in situ* hybridization on somite-matched embryos as previously described (Holmes and Niswander, 2001). Probes used were: mouse *Axin2*, mouse *Lef1* and mouse *Pax3* (all probes generously provided by L.A.N.'s lab). The RNA *in situ* hybridization probes used were digoxigenin-labeled probes recognized by anti-digoxigenin antibodies conjugated with alkaline phosphatase (Sigma-Aldrich, 11093724910). Upon incubation with the chromogenic substrate, purple color develops that in turn indicates the expression of the specific gene in that tissue (BM-purple, Sigma-Aldrich, 11442074001). Photos were taken using the Nikon SMZ18 Stereoscope with Nikon DS-Ri1 CCD-cooled camera with the 3× objective.

Whole-mount β-galactosidase staining and sectioning

β-Galactosidase staining of whole-mount embryos was performed as previously described (Heffner et al., 2012). Briefly, following fixation, E9.5 and E12.5 embryos were washed and permeabilized in detergent and incubated overnight at 37°C in 1 mg/ml X-gal staining solution, then fixed in 4% PFA in 1× PBS at 4°C overnight. X-gal-stained $Snx3^{+/-}$ embryos were imaged on a Leica M125 stereoscope using a 1× Planapo objective. E9.5 embryos were then embedded in OCT, sectioned at 20 µm and re-imaged using the Olympus IX83 Fluorescence Microscope.

TCF/Lef:H2B/EGFP reporter analysis

B6N(Cg)-$Snx3^{tm1.1(KOMP)Vlcg}$/mice were crossed with the STOCK Tg(TCF/Lef1-HIST1H2BB/EGFP)61Hadj/J (Stock #013752) WNT reporter strain to produce heterozygous *Snx3* knockout animals carrying the H2B-EGFP transgene. Female $Snx3^{+/-}$ animals were crossed with $Snx3^{+/-}$/*H2B-EGFP*$^{Tg/0}$ males. Embryos were dissected at E8.5 and fixed in 4% PFA for 30 min, rinsed in 1× PBS and genotyped. $Snx3^{+/+}$/*H2B-EGFP*$^{Tg/0}$ and $Snx3^{-/-}$/*H2B-EGFP*$^{Tg/0}$ embryos were imaged using a Leica M165 FC Fluorescence Microscope with a 1× Planapo objective. A 350 ms exposure time and gain setting of 1 were used for image capture. E8.5 embryos were then embedded in OCT, sectioned at 20 µm and imaged on the Nikon Structured Illumination Super-resolution and A1 Laser Scanning Confocal Microscope with a 20× objective.

Length-to-width ratios

Embryos were carefully dissected at E8.5, fixed in 4% PFA overnight, rinsed in 1× PBS, imaged on Olympus IX83 Fluorescence Microscope with the 4× objective or the Nikon SMZ18 Stereoscope with Nikon DS-Ri1 CCD-cooled camera with the 3× objective, and measured using ImageJ.

MEF production and maintenance

Heterozygous B6N(Cg)-Snx3tm1.1(KOMP)Vlcg/J were housed together and observance of the vaginal plug was considered to be 0.5 days post conception. Embryos were dissected from the dam at embryonic day 11.5 and 12.5 to make mouse embryonic fibroblast (MEF) primary culture cells. The head and internal organs were discarded, and the remaining embryonic tissue was dissociated in 3 ml 0.25% Trypsin/EDTA 1× (Gibco Life Technologies, 25200-056) at 37°C for 5 min. 5 ml of the total mixture of DMEM/10% FBS/1% GlutaMAX/1% Pen Strep (Gibco Life Technologies, 11995-065, A3160601, 35050061, 15140163) was added to each sample and spun down at 1968 ***g*** for 5 min. Supernatant was aspirated off and the pellet was resuspended in 3 ml of a mixture of DMEM/10% FBS/1% GlutaMAX/1% Pen Strep and plated into a 12-well dish or a 6-well dish (Costar, 3513 or 3516), plating one embryo per well. Cells were incubated

Development (2020) 147, dev192518. doi:10.1242/dev.192518

overnight and media was changed the following day. Cells were expanded into larger dishes until they reached passage 2 or 3. Yolk sacs from each embryo were genotyped as described above and cells were stored frozen in DMEM/10%FBS/1%GlutaMAX/1%Pen Strep with 10% DMSO (Sigma-Aldrich, 472301) in liquid nitrogen.

Plasmid construction

Snx3-gfp was made using mouse-tagged ORF clone (NM_017472, Origene, MR215963) and pCMV6-AC-GFP (Origene, PS100010) both separately digested with SgfI and MluI (New England Biosciences) to extract the *Snx3* reading frame and linearize, respectively. Digests were run on a 1% agarose gel and the *Snx3* insert (495 bp) and linearized pCMV6-AC-GFP (6551 base pairs) were gel extracted using Zymoclean Gel DNA Recovery Kit #D4008) and ligated together in a 3:1 ratio using Takara Clontech DNA ligation kit version 2.1 (6022). The ligation reaction was transformed using Takara Stellar competent cells (636736), plated on ampicillin-resistant plates, and single clones were picked to inoculate cultures overnight and then midi-prepped using Zyppy Plasmid Midiprep kit (D4200). Plasmids were sequenced by Quintarabio using in house VP1.5 and XL39 primers. *Snx3-rfp* was made following the same protocol, except using pCMV6-AC-RFP (Origene, PS100034).

SNX3-p.Asn35Lys-GFP was made via site-directed mutagenesis of the previously described *Snx3-gfp* plasmid using QuickChange Lightning Multi Site-Directed Mutagenesis Kit (Agilent Technologies #2105-15-5) according to the manufacturer's protocol. Plasmids were sequenced by Quintarabio using in house VP1.5 and XL39 primers to confirm successful mutagenesis: mutagenesis forward primer, 5′-TCG CGA TCG ACG TGA GCA AAC CGC AGA CCG-3′; mutagenesis reverse primer, 5′-CGG TCT GCG GTT TGC TCA CGT CGA TCT CGA-3′.

Wls-rfp was made using mouse tagged ORF clone (NM_026582, Origene, M208639) and pCMV6-AC-RFP (Origene, PS100034) both separately digested with SgfI and MluI (New England Biosciences) to extract the *Wls* reading frame and linearize, respectively. Digests were run on a 1% agarose gel and the *Wls* insert (1623 bp) and linearized pCMV6-AC-RFP (6600 bp) were gel extracted, ligated and clones selected as above. Plasmids were sequenced by Quintarabio using in house VP1.5 and XL39 primers.

Rab5-BFP, *Lamp1-BFP* and *Lamp1-GFP* were generously gifts from the lab of Dr Gia Voeltz (University of Colorado at Boulder, CO, USA). Mouse *Wnt1-gfp* ORF tagged clone was from Origene (MG205702). Mouse *Wnt5a-rfp* was generously provided by Bin Li (University of Colorado at Boulder, CO, USA).

Enzyme-linked immunosorbent assays for WNT1 and WNT5A

WNT1

50,000 MEFs were plated in 24-well plates (Costar #3526). Wild-type and $Snx3^{-/-}$ cells were transfected with 0.5 µg *Wnt1-gfp* plasmid and 0.5 µg *pCMV6-AC-RFP* as a transfection control. For the rescue, $Snx3^{-/-}$ cells were transfected with 0.5 µg *Snx3-rfp* and 0.5 µg *Wnt1-gfp*. Wild type represents three biological replicates containing respective technical replicates of n=6, n=3 and n=2, for a total of n=11 data points. $Snx3^{-/-}$ represents three biological replicates containing respective technical replicates of n=2, n=3 and n=5, for a total of 10 data points. $Snx3^{-/-}$+wild-type *Snx3* (rescue) represents three biological replicates containing respective technical replicates of n=2, n=3 and n=6, for a total of 11 data points.

WNT5A

50,000 MEFs were plated in 24-well plates (Costar, 3526). Wild-type and $Snx3^{-/-}$ cells were transfected with 0.5 µg *Wnt5a-rfp* plasmid and 0.5 µg *pCMV6-AC-GFP* as a transfection control. For the rescue, $Snx3^{-/-}$ cells were transfected with 0.5 µg *Snx3-gfp* and 0.5 µg *Wnt5a-rfp*. Wild type represents three biological replicates containing respective technical replicates of n=8, n=2 and n=2, for a total of n=12 data points. $Snx3^{-/-}$ represents four biological replicates containing respective technical replicates of n=8, n=2, n=2 and n=3 for a total of 15 data points. $Snx3^{-/-}$+wild-type *Snx3* represents three biological replicates containing respective technical replicates of n=1, n=2 and n=3, for a total of six data points.

All cells were seeded at identical cell densities and transfected with equal amounts of plasmid from master mix and performed in parallel. All transfections were performed using Xfect transfection kit according to manufacturer's protocol (Takara Clontech, 631317). Media were collected 24 h post-transfection using Eppendorf LoBind Microcentrifuge Tubes (22431081). Media were spun down for 10 min at 27,670 ***g*** and the supernatant was transferred to a new LoBind tube and diluted 1:3 with the sample diluent provided in the respective kit. The media from each condition was subject to the ELISA kit according to the manufacturer's protocol (mouse WNT1 ELISA, Antibodies Online ABIN1153029; mouse WNT5A ELISA, Antibodies Online, ABIN837310). The absorbance was read at 450 nm using the Synergy 2 Multi-Mode Microplate Reader. Graphs show three independent experiments and all individual data points.

Transfection and live cell imaging of MEFs

Cells from embryos were isolated as described above, then counted using a hemocytometer, 300,000 cells seeded into 35 mm glass-bottom plates (MatTek, P35G-1.5-14-C) and incubated for 24 h. Wild-type MEFs were transfected with *Snx3-gfp+Wls-rfp*, *Rab5-bfp+Wls-rfp* or *Lamp1-bfp+Wls-rfp*. $Snx3^{-/-}$ MEFs were transfected with *Rab5-bfp+Wls-rfp* or *Lamp1-bfp+Wls-rfp*. For the rescue condition, $Snx3^{-/-}$ MEFs were transfected with *Snx3-gfp+Rab5-bfp+Wls-rfp* or *Snx3-gfp+Lamp1-bfp+Wls-rfp*. For the transfection of the plasmid containing the human mutation, $Snx3^{-/-}$ MEFs were transfected with *SNX3-p.Asn35Lys-GFP+Wls-rfp*. Up to 3 µg total plasmid was transfected for each condition. All cells treated with bafilomycin were seeded and processed identically up to the drug treatment step. All transfections were carried out using the Xfect transfection kit according to manufacturer's protocol (Takara Clontech, 631317). For the Bafilomycin treatment, cells were cultured in 100 nm bafilomycin A1 (Fisher Scientific, 501031771) for 3 h and immediately imaged. All cells were imaged 24 h post-transfection, in a humidified chamber with 5% CO_2 on the Cell Voyager CV1000 scanning disk confocal system at the University of Colorado Boulder microscopy core. Cells were imaged using the 40× oil immersion lens (0.1915 µm/pixel), with image acquisition every 10 s, up to 100 times for each cell. The excitation, exposures and gain were set within the same range of values across biological samples. Statistics represent three independent experiments of three biological replicates containing three technical replicates for each condition. Colocalization analysis and total fluorescence quantification was performed using ImageJ.

Whole-exome human data

Whole exome sequencing of a cohort of 511 myelomeningocele affected sporadic individuals recruited from spina bifida clinics from multiple sites in Texas, California, Kentucky and Ontario underwent whole-exome sequencing in order to identify potential mutations that could contribute to the NTD. Whole-exome sequencing was performed using the Ion Proton platform following the manufacturer's standard protocols. The total read depth was 62 with 37 Ts and 25 Cs. Torrent Suite software was used for sequence mapping and sequence analysis with reference to GRCh37/hg19 (Life Technologies/Fisher Scientifics). Variants that passed standard Variant Quality Score Recalibration filters following the Genome Analysis Toolkit HaplotypeCaller best practices workflows were retained for further analyses (Van der Auwera et al., 2013). Additional hard filters (alternate allele depth ≥25% and genotype quality ≥20, excess heterozygosity ≤56) were applied to minimize false-positive variant calls. A missense point mutation identified was in the *SNX3* gene in one individual resulting in a G-to-T transversion in exon 1 (GRCh37/hg19 6:108582021:G:T with G allele read depth of 49 and T allele read depth of 40), creating an asparagine-to-lysine amino acid change (p.Asn35Lys).

Lithium chloride intraperitoneal injections

Heterozygous male and females were housed together, and observance of the vaginal plug was considered 0.5 days post-conception. Pregnant females were intraperitoneally injected with 300 µl of 150 mM lithium chloride at E7.5 and E8.5. Embryos were dissected at E10.5 and washed in 4% paraformaldehyde at 4°C overnight. The embryos were genotyped and imaged using the Olympus IX83 Fluorescence Microscope. Three independent litters were dissected.

Development (2020) 147, dev192518. doi:10.1242/dev.192518

Quantifications and statistical analyses

Total GFP fluorescence in the *TCF/Lef:H2B-GFP* reporter wild-type and *Snx3*$^{-/-}$ E8.5 embryos was measured using ImageJ and background was subtracted. An unpaired *t*-test with Welch's correction was performed to test for significance. Graphs show individual data points and mean±s.e.m. plotted using Graphpad Prism software.

Length-to-width ratios were calculated using ImageJ with the 'line draw' tool to trace the length and the width of each wild-type (n=10) or *Snx3*$^{-/-}$ (n=9) E8.5 embryo. The means for each genotype were calculated and a two-tailed *t*-test was performed to test for statistical significance using Graphpad Prism software. Data are mean±s.e.m. and were plotted using Graphpad Prism software.

Quantification of the ELISAs was performed using Graphpad Prism software to calculate the means of the absorbance reading at 450 nm for each experimental condition, then performing a two tailed *t*-test to test for statistical significance. Data are mean±s.e.m. and were plotted using Graphpad Prism software.

Colocalization analysis for live-cell imaging was quantified using the Colocalization plug-in by ImageJ. Briefly, the images were loaded to ImageJ, channels were merged to create an 8-bit TIFF, then fluorescent channels were split and auto-thresholded for pixel intensity. Then the Colocalization plug-in was employed to calculate the percent overlap between pixels of each channel, indicating overlap of fluorescent proteins within the frame (imagej.net). Statistical analysis was performed using Graphpad Prism Software for two-tailed *t*-tests to test for statistical differences in pixel overlap of each experimental condition. Data are mean±s.e.m. and were plotted using Graphpad Prism software.

Quantification of total WLS fluorescence in all conditions was performed using ImageJ with the background subtracted and normalized for area. Statistical analysis was performed using Graphpad Prism software using two-tailed *t*-tests or non-parametric *t*-tests for data without normal distribution, to test for statistically significant differences in total WLS fluorescence. Individual data points and mean±s.e.m. were plotted using Graphpad Prism software.

Fishers exact test was performed using Graphpad Prism to evaluate the statistical significance of the rescued *Snx3*$^{-/-}$ embryos treated with LiCl compared with the *Snx3*$^{-/-}$ embryos not rescued by LiCl. Power calculations were performed to identify the smallest number of animals required for adequate detection of effect size. The B6N(Cg)-Snx3tm1.1(KOMP)Vlcg/J mouse shows a classic Mendelian ratio for all genotypes and the *Snx3*$^{-/-}$ mice show a 100% penetrant NTD phenotype. All datasets were tested for normality using Graphpad Prism and P<0.05 was considered significant for all experiments. The pre-established exclusion criteria were that any single data point three standard deviations from the mean was considered an outlier and not included in analysis.

Acknowledgements

We thank the members of L.A.N.'s lab for the help and feedback throughout the course of these experiments, especially Lori Bulwith who helped with mouse husbandry. We also thank CU Boulder undergraduate student Megan Hupka for help with mouse dissections, MEF production and transfections, as well as CU Boulder undergraduate student Caitlin Ryan for help with genotyping and mouse dissections. We thank the CU Boulder Office for Animal Resources staff for help with colony care and training on intraperitoneal injections. We thank the University of Colorado Boulder Light Microscopy Core Facility and Dr James Orth, PhD for assistance with the CellVoyager CV1000 Yokogawa spinning disk confocal microscope for all live-cell imaging, University of Colorado Boulder Stem Cell Research and Technology Core and Dr Teisha Rowland, PhD for the use of the Olympus IX83 Fluorescence Microscope for whole embryo imaging, and the University of Colorado Anschutz Medical Campus laboratory of Dr Julie Siegenthaler, PhD for the use of the Nikon SMZ18 Stereoscope with Nikon DS-Ri1 CCD-cooled camera to image whole-mount RNA *in situ* hybridization embryos.

Competing interests

The authors declare no competing or financial interests.

Author contributions

Conceptualization: H.M.B., L.A.N.; Methodology: H.M.B., L.A.N.; Validation: H.M.B.; Formal analysis: H.M.B.; Investigation: H.M.B., L.A.N.; Resources: H.M.B., L.A.N., S.A.M., H.N., K.S.A.; Data curation: H.M.B., H.N., K.S.A.; Writing - original draft: H.M.B.; Writing - review & editing: H.M.B., L.A.N., S.A.M., H.N., K.S.A.; Visualization: H.M.B.; Supervision: H.M.B., L.A.N.; Project administration: H.M.B., L.A.N.; Funding acquisition: L.A.N.

Funding

This work was supported by the National Institutes of Health Eunice Kennedy Shriver National Institute of Child Health and Human Development (HD081562 to L.A.N. with co-PIs Trevor Williams and David Clouthier, University of Colorado Anschutz Medical Campus; and HD073434 to K.S.A.). Deposited in PMC for release after 12 months.

Supplementary information

Supplementary information available online at
https://dev.biologists.org/lookup/doi/10.1242/dev.192518.supplemental

References

Allache, R., Wang, M., De Marco, P., Merello, E., Capra, V. and Kibar, Z. (2015). Genetic studies of ANKRD6 as a molecular switch between Wnt signaling pathways in human neural tube defects. *Birth Defects Res. A Clin. Mol. Teratol.* **103**, 20-26. doi:10.1002/bdra.23273

Anderson, M. J., Schimmang, T. and Lewandoski, M. (2016). An FGF3-BMP signaling axis regulates caudal neural tube closure, neural crest specification and anterior-posterior axis extension. *PLoS Genet.* **12**, e1006018. doi:10.1371/journal.pgen.1006018

Au, K. S., Ashley-Koch, A. and Northrup, H. (2010). Epidemiologic and genetic aspects of spina bifida and other neural tube defects. *Dev. Disab. Res. Rev.* **16**, 6-15. doi:10.1002/ddrr.93

Belenkaya, T. Y., Wu, Y., Tang, X., Zhou, B., Cheng, L., Sharma, Y. V., Yan, D., Selva, E. M. and Lin, X. (2008). The retromer complex influences Wnt secretion by recycling wntless from endosomes to the trans-Golgi network. *Dev. Cell* **14**, 120-131. doi:10.1016/j.devcel.2007.12.003

Carter, M., Chen, X., Slowinska, B., Minnerath, S., Glickstein, S., Shi, L., Campagne, F., Weinstein, H. and Ross, M. E. (2005). Crooked tail (Cd) model of human folate-responsive neural tube defects is mutated in Wnt coreceptor lipoprotein receptor-related protein 6. *Proc. Natl. Acad. Sci. USA* **102**, 12843-12848. doi:10.1073/pnas.0501963102

Castranio, T. and Mishina, Y. (2009). BMP2 is required for cephalic neural tube closure in the mouse. *Dev. Dyn.* **238**, 110-122. doi:10.1002/dvdy.21829

Chen, C., Garcia-Santos, D., Ishikawa, Y., Seguin, A., Li, L., Fegan, K. H., Hildick-Smith, G. J., Shah, D. I., Cooney, J. D., Chen, W. et al. (2013). Snx3 regulates recycling of the transferrin receptor and iron assimilation. *Cell Metab.* **17**, 343-352. doi:10.1016/j.cmet.2013.01.013

Cui, Y., Carosi, J. M., Yang, Z., Ariotti, N., Kerr, M. C., Parton, R. G., Sargeant, T. J. and Teasdale, R. D. (2019). Retromer has a selective function in cargo sorting via endosome transport carriers. *J. Cell Biol.* **218**, 615-631. doi:10.1083/jcb.201806153

Cullen, P. J. and Steinberg, F. (2018). To degrade or not to degrade: mechanisms and significance of endocytic recycling. *Nat. Rev. Mol. Cell Biol.* **19**, 679-696. doi:10.1038/s41580-018-0053-7

Delevoye, C., Miserey-Lenkei, S., Montagnac, G., Gilles-Marsens, F., Paul-Gilloteaux, P., Giordano, F., Waharte, F., Marks, M. S., Goud, B. and Raposo, G. (2014). Recycling endosome tubule morphogenesis from sorting endosomes requires the kinesin motor KIF13A. *Cell Rep.* **6**, 445-454. doi:10.1016/j.celrep.2014.01.002

Fu, J., Ivy Yu, H.-M., Maruyama, T., Mirando, A. J. and Hsu, W. (2011). Gpr177/mouse Wntless is essential for Wnt-mediated craniofacial and brain development. *Dev. Dyn.* **240**, 365-371. doi:10.1002/dvdy.22541

Gao, B. (2012). Wnt Regulation of Planar Cell Polarity (PCP). *Curr. Top. Dev. Biol.* **101**, 263-295. doi:10.1016/B978-0-12-394592-1.00008-9

Goodman, R. M., Thombre, S., Firtina, Z., Gray, D., Betts, D., Roebuck, J., Spana, E. P. and Selva, E. M. (2006). Sprinter: A novel transmembrane protein required for Wg secretion and signaling. *Development* **133**, 4901-4911. doi:10.1242/dev.02674

Haft, C. R., De La Luz Sierra, M., Barr, V. A., Haft, D. H. and Taylor, S. I. (1998). Identification of a family of sorting nexin molecules and characterization of their association with receptors. *Mol. Cell. Biol.* **18**, 7278-7287. doi:10.1128/MCB.18.12.7278

Harris, M. J. and Juriloff, D. M. (2007). Mouse mutants with neural tube closure defects and their role in understanding human neural tube defects. *Birth Defects Res. A Clin. Mol. Teratol.* **79**, 187-210. doi:10.1002/bdra.20333

Harterink, M., Port, F., Lorenowicz, M. J., Mcgough, I. J., Silhankova, M., Betist, M. C., Van Weering, J. R. T., Van Heesbeen, R. G. H. P., Middelkoop, T. C., Basler, K. et al. (2011). A SNX3-dependent retromer pathway mediates retrograde transport of the Wnt sorting receptor Wntless and is required for Wnt secretion. *Nat. Cell Biol.* **13**, 914-923. doi:10.1038/ncb2281

Heffner, C. S., Herbert Pratt, C., Babiuk, R., Sharma, Y., Rockwood, S. F., Donahue, L. R., Eppig, J. T. and Murray, S. A. (2012). Supporting conditional

mouse mutagenesis with a comprehensive cre characterization resource. *Nat. Commun.* **3**, 1218. doi:10.1038/ncomms2186.
Holmes, G. and Niswander, L. (2001). Expression of slit-2 and slit-3 during chick development. *Dev. Dyn.* **222**, 301-307. doi:10.1002/dvdy.1182
Ikeya, M., Lee, S. M. K., Johnson, J. E., Mcmahon, A. P. and Takada, S. (1997). Wnt signalling required for expansion of neural crest and cns progenitors. *Nature* **389**, 966-970. doi:10.1038/40146
Johannes, L. and Wunder, C. (2011). The SNXy flavours of endosomal sorting. *Nat. Cell Biol.* **13**, 884-886. doi:10.1038/ncb2300
Juriloff, D. M. and Harris, M. J. (2012). A consideration of the evidence that genetic defects in planar cell polarity contribute to the etiology of human neural tube defects. *Birth Defects Res. A Clin. Mol. Teratol.* **94**, 824-840. doi:10.1002/bdra.23079
Juriloff, D. and Harris, M. (2018). Insights into the etiology of mammalian neural tube closure defects from developmental, genetic and evolutionary studies. *J. Dev. Biol.* **6**, 22. doi:10.3390/jdb6030022
Kanzler, B., Foreman, R. K., Labosky, P. A. and Mallo, M. (2000). BMP signaling is essential for development of skeletogenic and neurogenic cranial neural crest. *Development* **127**, 1095-1104.
Klein, P. S. and Melton, D. A. (1996). A molecular mechanism for the effect of lithium on development. *Proc. Natl. Acad. Sci. USA* **93**, 8455-8459. doi:10.1073/pnas.93.16.8455
Komiya, Y. and Habas, R. (2008). Wnt signal transduction pathways. *Organogenesis* **4**, 68-75. doi:10.4161/org.4.2.5851
Lenoir, M., Ustunel, C., Rajesh, S., Kaur, J., Moreau, D., Gruenberg, J. and Overduin, M. (2018). Phosphorylation of conserved phosphoinositide binding pocket regulates sorting nexin membrane targeting. *Nat. Commun.* **9**, 993. doi:10.1038/s41467-018-03370-1
Li, F., Liu, C.-F., Xu, Y.-M., Guo, Y.-L., Xue, S.-W., Kong, X.-D., Zhang, H.-B., Zhang, Y. and Kang, J.-S. (2018). Neonatal lethality and recycling defect of transferrin receptor in mice with Syntaxin12/13 disruption. *Protein Cell* **10**, 67-71. doi:10.1007/s13238-018-0519-6
Logan, C. Y. and Nusse, R. (2004). The Wnt signaling pathway in development and disease. *Annu. Rev. Cell Dev. Biol.* **20**, 781-810. doi:10.1146/annurev.cellbio.20.010403.113126
Lucas, M., Gershlick, D. C., Vidaurrazaga, A., Rojas, A. L., Bonifacino, J. S. and Hierro, A. (2016). Structural mechanism for cargo recognition by the retromer complex. *Cell* **167**, 1623-1635.e14. doi:10.1016/j.cell.2016.10.056
McGough, I. J., De Groot, R. E. A., Jellett, A. P., Betist, M. C., Varandas, K. C., Danson, C. M., Heesom, K. J., Korswagen, H. C. and Cullen, P. J. (2018). SNX3-retromer requires an evolutionary conserved MON2:DOPEY2:ATP9A complex to mediate Wntless sorting and Wnt secretion. *Nat. Commun.* **9**, 3737. doi:10.1038/s41467-018-06114-3
Merte, J., Jensen, D., Wright, K., Sarsfield, S., Wang, Y., Schekman, R. and Ginty, D. D. (2010). Sec24b selectively sorts Vangl2 to regulate planar cell polarity during neural tube closure. *Nat. Cell Biol.* **12**, 41-46. doi:10.1038/ncb2002
Milunsky, A., Jick, H., Jick, S. S., Bruell, C. L., MacLaughlin, D. S., Rothman, K. J. and Willett, W. (1989). Multivitamin/Folic acid supplementation in early pregnancy reduces the prevalence of neural tube defects. *J. Am. Med. Assoc.* **262**, 2847-2842. doi:10.1001/jama.1989.03430200091032
Misra, K. and Matise, M. P. (2010). A critical role for sFRP proteins in maintaining caudal neural tube closure in mice via inhibition of BMP signaling. *Dev. Biol.* **337**, 74-83. doi:10.1016/j.ydbio.2009.10.015
Murdoch, J. N. and Copp, A. J. (2010). The relationship between sonic hedgehog signaling, cilia, and neural tube defects. *Birth Defects Res. A Clin. Mol. Teratol.* **88**, 633-652. doi:10.1002/bdra.20686
Nusse, R., Brown, A., Papkoff, J., Scambler, P., Shackleford, G., Mcmahon, A., Moon, R. and Varmus, H. (1991). A new nomenclature for int-1 and related genes: The Wnt gene family. *Cell* **64**, 231. doi:10.1016/0092-8674(91)90633-A
Perry, W. L., 3rd, Vasicek, T. J., Lee, J. J. Rossi, J. M., Zeng, L., Zhang, T., Tilghman, S. M. and Costantini, F. (1995). Phenotypic and molecular analysis of a transgenic insertional allele of the mouse fused locus. *Genetics* **141**, 321-332.
Qian, D., Jones, C., Rzadzinska, A., Mark, S., Zhang, X., Steel, K. P., Dai, X. and Chen, P. (2007). Wnt5a functions in planar cell polarity regulation in mice. *Dev. Biol.* **306**, 121-133. doi:10.1016/j.ydbio.2007.03.011
Ray, H. J. and Niswander, L. (2012). Mechanisms of tissue fusion during development. *Development* **139**, 1701-1711. doi:10.1242/dev.068338
Singla, A., Fedoseienko, A., Giridharan, S. S. P., Overlee, B. L., Lopez, A., Jia, D., Song, J., Huff-Hardy, K., Weisman, L., Burstein, E. et al. (2019). Endosomal PI(3)P regulation by the COMMD/CCDC22/CCDC93 (CCC) complex controls membrane protein recycling. *Nat. Commun.* **10**, 4271. doi:10.1038/s41467-019-12221-6
Song, L., Li, Y., Wang, K., Wang, Y.-Z., Molotkov, A., Gao, L., Zhao, T., Yamagami, T., Wang, Y., Gan, Q. et al. (2009). Lrp6-mediated canonical Wnt signaling is required for lip formation and fusion. *Development* **136**, 3161-3171. doi:10.1242/dev.037440
Stokes, B. A., Sabatino, J. A. and Zohn, I. E. (2016). High levels of iron supplementation prevents neural tube defects in the Fpn1^{ffe} mouse model. *Birth Defects Res. A Clin. Mol. Teratol* **109**, 81-91. doi:10.1002/bdra.23542
Sun, J., Yu, S., Zhang, X., Capac, C., Aligbe, O., Daudelin, T., Bonder, E. M. and Gao, N. (2017). A Wntless-SEC12 complex on the ER membrane regulates early Wnt secretory vesicle assembly and mature ligand export. *J. Cell Sci.* **130**, 2159-2171. doi:10.1242/jcs.200634
Van Der Auwera, G. A., Carneiro, M. O., Hartl, C., Poplin, R., Del Angel, G., Levy-Moonshine, A., Jordan, T., Shakir, K., Roazen, D., Thibault, J. et al. (2013). From fastQ data to high-confidence variant calls: the genome analysis toolkit best practices pipeline. *Curr. Protoc. Bioinform.* **43**, 11.10.1-11.10.33. doi:10.1002/0471250953.bi1110s43
Wang, J. (2006). Dishevelled genes mediate a conserved mammalian PCP pathway to regulate convergent extension during neurulation. *Development* **133**, 1767-1778. doi:10.1242/dev.02347
Wang, Y., Song, L. and Zhou, C. J. (2010). The canonical Wnt/β-catenin signaling pathway regulates Fgf signaling for early facial development. *Dev. Biol.* **349**, 250-260. doi:10.1016/j.ydbio.2010.11.004
Wang, J., Fedoseienko, A., Chen, B., Burstein, E., Jia, D. and Billadeau, D. D. (2018). Endosomal receptor trafficking: Retromer and beyond. *Traffic* **19**, 578-590. doi:10.1111/tra.12574
Wilde, J. J., Petersen, J. R. and Niswander, L. (2014). Genetic, Epigenetic, and Environmental Contributions to Neural Tube Closure. *Annu. Rev. Genet.* **48**, 583-611. doi:10.1146/annurev-genet-120213-092208
Worby, C. A. and Dixon, J. E. (2002). Sorting out the cellular functions of sorting nexins. *Nat. Rev. Mol. Cell Biol.* **3**, 919-931. doi:10.1038/nrm974
Xu, Y., Hortsman, H., Seet, L., Wong, S. H. and Hong, W. (2001). SNX3 regulates endosomal function through its PX-domain-mediated interaction with PtdIns(3)P. *Nat. Cell Biol.* **3**, 658-666. doi:10.1038/35083051
Yang, X.-Y., Zhou, X.-Y., Wang, Q. Q., Li, H., Chen, Y., Lei, Y.-P., Ma, X.-H., Kong, P., Shi, Y., Jin, L. et al. (2013). Mutations in the COPII vesicle component gene SEC24B are associated with human neural tube defects. *Hum. Mutat.* **34**, 1094-1101. doi:10.1002/humu.22338
Ybot-Gonzalez, P., Cogram, P., Gerrelli, D. and Copp, A. J. (2002). Sonic hedgehog and the molecular regulation of mouse neural tube closure. *Development* **129**, 2507-2517.
Ybot-Gonzalez, P., Savery, D., Gerrelli, D., Signore, M., Mitchell, C. E., Faux, C. H., Greene, N. D. E. and Copp, A. J. (2007). Convergent extension, planar-cell-polarity signalling and initiation of mouse neural tube closure. *Development* **134**, 789-799. doi:10.1242/dev.000380
Yu, J., Chia, J., Canning, C. A., Jones, C. M., Bard, F. A. and Virshup, D. M. (2014). WLS Retrograde transport to the endoplasmic reticulum during Wnt secretion. *Dev. Cell* **29**, 277-291. doi:10.1016/j.devcel.2014.03.016
Zaganjor, I., Sekkarie, A., Tsang, B. L., Williams, J., Razzaghi, H., Mulinare, J., Sniezek, J. E., Cannon, M. J. and Rosenthal, J. (2016). Describing the prevalence of neural tube defects worldwide: a systematic literature review. *PLoS ONE* **11**, e0151586. doi:10.1371/journal.pone.0151586
Zhang, P., Wu, Y., Belenkaya, T. Y. and Lin, X. (2011). SNX3 controls Wingless/Wnt secretion through regulating retromer-dependent recycling of Wntless. *Cell Res.* **21**, 1677-1690. doi:10.1038/cr.2011.167
Zhao, T., Gan, Q., Stokes, A., Lassiter, R. N. T., Wang, Y., Chan, J., Han, J. X., Pleasure, D. E., Epstein, J. A. and Zhou, C. J. (2014). β-catenin regulates Pax3 and Cdx2 for caudal neural tube closure and elongation. *Development (Camb.)* **141**, 148-157. doi:10.1242/dev.101550
Zhou, C.-Z., Li De La Sierra-Gallay, I., Quevillon-Cheruel, S., Collinet, B., Minard, P., Blondeau, K., Henckes, G., Aufrère, R., Leulliot, N., Graille, M. et al. (2003). Crystal structure of the yeast Phox Homology (PX) domain protein Grd19p complexed to phosphatidylinositol-3-phosphate. *J. Biol. Chem.* **278**, 50371-50376. doi:10.1074/jbc.M304392200
Zohn, I. E., De Domenico, I., Pollock, A., Ward, D. M. V., Goodman, J. F., Liang, X., Sanchez, A. J., Niswander, L. and Kaplan, J. (2007). The flatiron mutation in mouse ferroportin acts as a dominant negative to cause ferroportin disease. *Blood* **109**, 4174-4180. doi:10.1182/blood-2007-01-066068

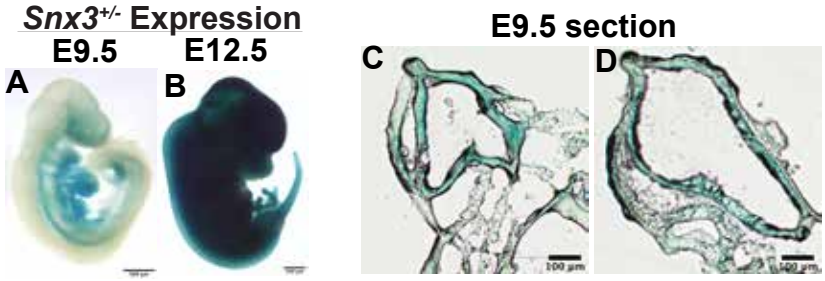

Figure S1. Snx3 is expressed in the neural tube of E9.5 embryos and expressed ubiquitously in E12.5 embryos. LacZ staining was performed on heterozygous embryos at E9.5 (n=2) and E12.5 (n=2) to visualize *Snx3* expression utilizing LacZ knocked into the *Snx3* locus. (A) *Snx3* expression in neural tube, and more strongly in neural derivatives and heart in E9.5 embryo. (B) *Snx3* ubiquitously expressed in E12.5 embryo. Scale bar represents 500 micrometers. (C, D) Strong *Snx3* expression in the neural epithelium of E9.5 embryos sectioned at 20 micrometers.

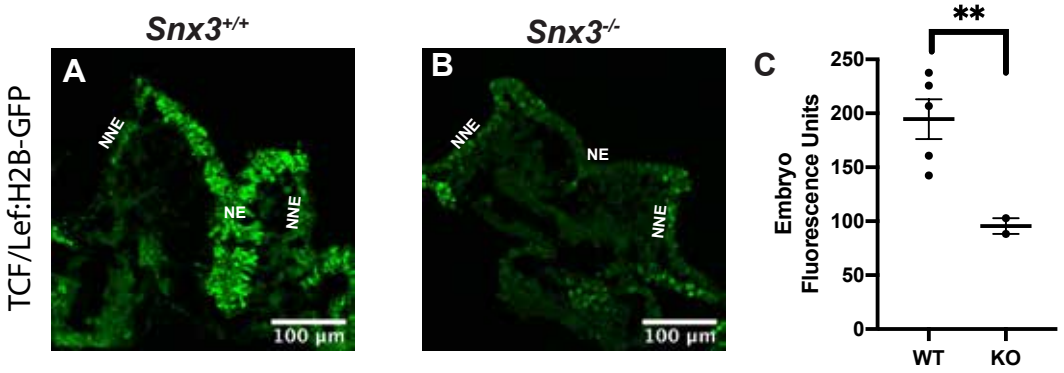

Figure S2. WNT activity is significantly decreased in the neural epithelium of E8.5 embryos. E8.5 embryos from TCF/Lef:H2B/GFP reporter mice were sectioned at 20 micrometer sections to visualize Wnt/β-cateninactivity in WT and *Snx3*$^{-/-}$ embryos. (A) Sectioned WT E.5 embryo showing strong WNT signaling activity in the cranial neural epithelium (NE). (B) Sectioned *Snx3*$^{-/-}$ E8.5 embryo showing loss of WNT signaling activity in the cranial neural epithelium, with no obvious change in the nonneural ectoderm (NNE). (C) The total fluorescence of whole mount E8.5 *Snx3*$^{-/-}$ embryos is statistically significantly lower than WT embryos, indicating less WNT activity (**p<0.01 by unpaired t-test with Welch's correction to test for statistical significance between the genotypes, n=5 for WT, n=2 for *Snx3*$^{-/-}$).

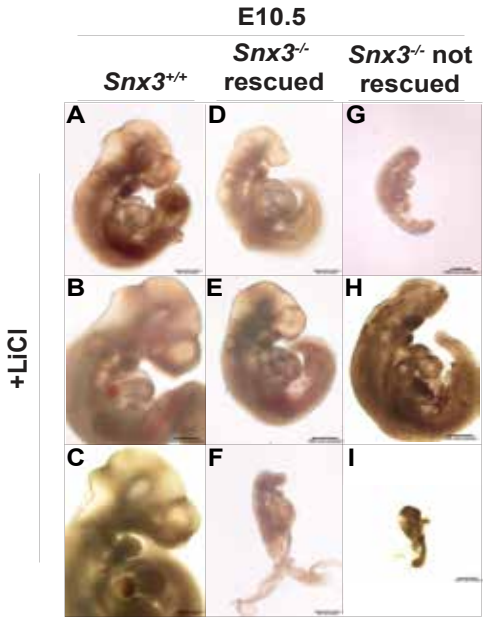

Figure S3. NTDs in Snx3$^{-/-}$ embryos can be rescued with LiCl. (A-C) E10.5 WT embryos from pregnant females intraperitoneally injected with 300 ul of 150 mM LiCl at E7.5 and E8.5 show normal neural tube closure. (D-F) E10.5 *Snx3*$^{-/-}$ embryos from pregnant females intraperitoneally injected with LiCl at E7.5 and E8.5 have closed their neural tube, indicating a full rescue of the cranial NTD (*p<0.05).
(G-I) E10.5 embryos in which the NTD was not rescued with LiCl treatment. Embryos are from 3 independent litters, WT n=6 and KO n=8, of which 4 showed a fully closed neural tube. Scale bar represents 500 micrometers.